Paper 34

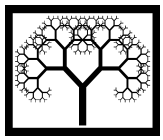

Proceedings of the First International Conference on
Railway Technology: Research, Development and Maintenance,
J. Pombo, (Editor),
Civil-Comp Press, Stirlingshire, Scotland

Enhanced Vehicle-Track Modelling: Methods, Models and Results

I. Kaiser
Institute of Robotics and Mechatronics
German Aerospace Center (DLR), Wessling, Germany

Abstract

For a more detailed description of the effects related to vehicle-track interaction, which are relevant for the running behaviour, for noise and for wear, refined models of the wheelset, the track and the wheel-rail contact are developed. The models for the wheelset and for the track take the structural dynamics of the wheelset and the rails into account. For the wheel-rail contact, an iterative solution based on a Boundary Element model is used. The investigation for the scenarios of undisturbed centred running and of permanent hunting shows a distinct influence of the structural flexibilities of the wheelsets and the track on the wheel-rail contact and on the running behaviour.

Keywords: vehicle-track interaction, flexible wheelset, flexible track, non-elliptic wheel-rail contact, structural dynamics, high-frequency behaviour, hunting.

1 Introduction and motivation

The interaction between vehicle and track is an important aspect in railway research: The running behaviour including stability and curving and thereby also the operational safety depend directly on the wheel-rail forces. Furthermore, irregularities of the running surfaces of wheel and rail excite structural vibrations. Such structural vibrations are especially relevant for noise, but have also an influence on durability and fatigue as well as on comfort. A third topic is the wear occurring in the wheel-rail contact, which has a strong impact on the maintenance effort and thereby on the economics of the entire vehicle-track system. The structural vibrations and the wear are not isolated phenomena, but linked to each other: The wear depends on the creepages in the contact, on which also structural vibrations can have an impact. In reverse, the wear can generate irregularities of the running surfaces, which excite structural vibra-

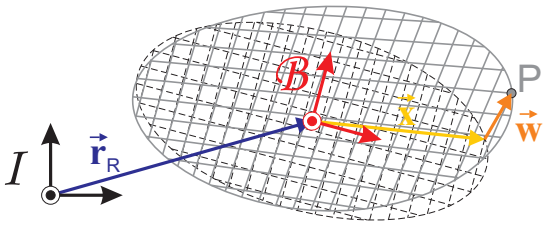

Figure 1: Kinematics for a particle of a flexible body.

tions. Therefore, an accurate modelling of the vehicle-track interaction including a refined modelling of the key components, which are the wheelsets, the track and the wheel-rail contact, is desirable.

2 Flexible wheelset

In a flexible multi-body system, the motions of a flexible body are usually described by a relative formulation. In this formulation, the motions of the undeformed body, which are also called rigid-body motions, and deformational motions are superposed. The translational rigid-body motions are expressed by a vector indicating the current position of a reference point R, e.g. the centre of gravity, while the rotational motions are expressed by the current orientation of the body-fixed frame $\mathcal{B}$. In the undeformed state, the position of a particle relative to the reference point is denoted by the vector $\mathbf{x}$. If this vector is expressed in the body-fixed frame, its time-derivative vanishes, i.e. $\frac{d\mathbf{x}^{\mathcal{B}}}{dt} = \mathbf{0}$. Due to the deformation, the particle is shifted from the reference position to the current position indicated by the point P, which is expressed by the vector $\mathbf{w}(\mathbf{x}, t)$. An overview of the kinematics is given in Figure 1. The current position of the particle can be expressed as:

$$\mathbf{r}_{\mathsf{P}}^{\mathcal{I}} = \mathbf{r}_{\mathsf{R}}^{\mathcal{I}}(t) + \mathbf{A}^{\mathcal{I}\mathcal{B}}(t) \left[\mathbf{x}^{\mathcal{B}} + \mathbf{w}^{\mathcal{B}}(\mathbf{x}^{\mathcal{B}}, t)\right] \tag{1}$$

The matrix $\mathbf{A}^{\mathcal{I}\mathcal{B}}(t)$ is the transformation matrix expressing the rotation between the inertial frame $\mathcal{I}$ and the body-fixed frame $\mathcal{B}$. – Usually, the deformations $\mathbf{w}^{\mathcal{B}}(\mathbf{x}^{\mathcal{B}}, t)$ of the flexible body are described by a modal synthesis. Here, shape functions $\mathbf{W}_i(\mathbf{x}^{\mathcal{B}})$ are scaled by time-dependent modal coordinates $q_i(t)$ and superposed, so that the deformation is described by:

$$\mathbf{w}^{\mathcal{B}}(\mathbf{x}^{\mathcal{B}}, t) = \sum_i \mathbf{W}_i(\mathbf{x}^{\mathcal{B}}) q_i(t) \tag{2}$$

The shape functions can be obtained by a Finite Element (FE) analysis. In many cases, eigenmodes of the flexible body are used as shape functions.

For the integration into a flexible multi-body system, the motions of the flexible body at the connections to other elements, e.g. force elements, are required. Here,

the main difficulty concerning the modelling of a wheelset as a flexible body arises: Due to the rolling motion, the wheel-rail forces are circulating around the wheel, i.e. the force-application point changes permanently. In the formulation (1) this means that the vector $\mathbf{x}^{\mathcal{B}}$ is no longer constant, but depends on time. Therefore, the current position of the particle, at which the wheel-rail forces act, is given by:

$$\mathbf{r}_{\mathsf{P}}^{\mathcal{I}} = \mathbf{r}_{\mathsf{R}}^{\mathcal{I}}(t) + \mathbf{A}^{\mathcal{I}\mathcal{B}}(t) \left[\mathbf{x}_{WR}^{\mathcal{B}}(t) + \sum_i \mathbf{W}_i(\mathbf{x}_{WR}^{\mathcal{B}}(t)) q_i(t) \right] \tag{3}$$

It has to be pointed out that the time-dependent vector $\mathbf{x}_{WR}^{\mathcal{B}}(t)$ does not describe any relative motion, but a change of the observed particle. As already mentioned, the shape functions are usually obtained by a FE analysis. The FE method is based on a discretisation using certain points, while the deformation field is described by local interpolation functions defined for each element. Thereby, the determination of the now time-dependent shape functions $\mathbf{W}_i(\mathbf{x}_{WR}^{\mathcal{B}}(t))$ requires a piecewise interpolation, which makes the evaluation very difficult.

Since the wheelset or at least the wheel rim is a rotational symmetric structure, it is obvious to use cylindrical coordinates, i.e. the radial coordinate r, the axial coordinate y and the azimut ϕ. Thereby, the vector $\mathbf{x}^{\mathcal{B}}$ can be expressed by

$$\mathbf{x}^{\mathcal{B}} = \begin{bmatrix} r\sin\phi & y & r\cos\phi \end{bmatrix}^T \tag{4}$$

In the case of the rotating wheelset, the azimut ϕ depends on time. The axial coordinate y and the radial coordinate r can be considered to be constant. The problem of the lateral shift of the wheel-rail contact will be discussed later. – Since the points $\mathbf{x}^{\mathcal{B}}(r,\phi,y)$ and $\mathbf{x}^{\mathcal{B}}(r,\phi+2\pi,y)$ denote the same particle, it is obvious to express the shape functions by a Fourier series:

$$\begin{aligned} \mathbf{x}^{\mathcal{B}} &= \begin{bmatrix} r\sin\phi & y & r\cos\phi \end{bmatrix}^T = \mathbf{x}^{\mathcal{B}}(r,\phi,y) \\ \Rightarrow \mathbf{W}_i(\mathbf{x}^{\mathcal{B}}) &= \mathbf{W}_i(r,\phi,y) = \sum_{k=0}^{N} \left[\mathbf{W}_{i,kC}(r,y)\cos(k\phi) + \mathbf{W}_{i,kS}(r,y)\sin(k\phi) \right] \end{aligned} \tag{5}$$

By this step, the interpolation using the local functions of the original FE model is avoided. The evaluation of a continuous function like the sine and the cosine function is more convenient. – In many cases, a railway wheelset is a perfectly rotational symmetric structure. The eigenmodes $\mathbf{W}_i$ of such a structure can be expressed in the following form:

$$\begin{aligned} \underbrace{\begin{bmatrix} U_i(r,\phi,y) \\ V_i(r,\phi,y) \\ W_i(r,\phi,y) \end{bmatrix}}_{\mathbf{W}_i(r,\phi,y)} &= \underbrace{\begin{bmatrix} \cos\phi & 0 & \sin\phi \\ 0 & 1 & 0 \\ -\sin\phi & 0 & \cos\phi \end{bmatrix}}_{\mathbf{A}_2(\phi)} \underbrace{\begin{bmatrix} T_i(r,\phi,y) \\ V_i(r,\phi,y) \\ R_i(r,\phi,y) \end{bmatrix}}_{\mathbf{U}_i(r,\phi,y)} \\ &= \mathbf{A}_2(\phi) \left[\mathbf{U}_{i,C}(r,y)\cos(k_i\phi) + \mathbf{U}_{i,S}(r,y)\sin(k_i\phi) \right] \end{aligned} \tag{6}$$

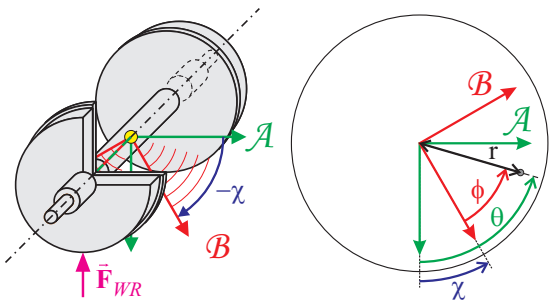

Figure 2: Body-fixed frame $\mathcal{B}$ and axle-fixed frame $\mathcal{A}$ of the rotating wheelset.

Here, the matrix $\mathbf{A}_2(\phi)$ expresses the transformation between the deformations U_i, V_i and W_i in the directions of Cartesian coordinates on the one hand and the deformations in the directions of the cylindrical coordinates on the other hand, i.e. the tangential deformation T_i, the radial deformation R_i and the axial deformation V_i. The eigenmode $\mathbf{U}_i$ expressed in cylindrical coordinates has one and only one periodicity k_i. Thereby, the Fourier series (5) describing the shape function $\mathbf{W}_i(r,\phi,y)$ contains only three terms having the periodicities $k = k_i - 1$, $k = k_i$ and $k = k_i + 1$. It can be shown that the expression

$$\mathbf{w} = \underbrace{\begin{bmatrix} \cos\phi & 0 & \sin\phi \\ 0 & 1 & 0 \\ -\sin\phi & 0 & \cos\phi \end{bmatrix}}_{\mathbf{A}_2(\phi)} \underbrace{\begin{bmatrix} \hat{T}_i(r,y)\sin(k_i\phi+\alpha_i) \\ \hat{V}_i(r,y)\cos(k_i\phi+\alpha_i) \\ \hat{R}_i(r,y)\cos(k_i\phi+\alpha_i) \end{bmatrix}}_{\mathbf{U}_i(r,\phi,y)} \cos(\omega_i t+\beta_i) \tag{7}$$

is a solution of Navier's equation, given e.g. in [1]. For a rotational symmetric structure, the density ρ, the shear modulus G and Poisson's ratio ν are independent of the azimut ϕ:

$$\Delta\mathbf{w} + \frac{1}{1-2\,\nu(r,y)}\mathbf{grad}\,\mathrm{div}\,\mathbf{w} - \frac{\rho(r,y)}{G(r,y)}\ddot{\mathbf{w}} = \mathbf{0} \tag{8}$$

A more convenient way of describing the rotating flexible wheelset can be achieved by introducing an intermediate axle-fixed frame $\mathcal{A}$, which performs all rigid body motions except the rolling motion χ, as displayed in Figure 2. In frame $\mathcal{A}$ the application point of the wheel-rail forces $\vec{\mathbf{F}}_{WR}$, which is indicated by the new azimut θ, is constant, i.e. $\theta = \phi(t) + \chi(t) = \mathrm{const}$. Now, a further simplification can be achieved by exploiting a further characteristic of the eigenmodes for a rotational symmetric structure: For $k_i \neq 0$ double eigenmodes expressing different spatial orientations occur, which can be formulated by:

$$\mathbf{U}_{i1}(r,\phi,y) = \mathbf{U}_{i,A}(r,y)\cos(k_i\phi) + \mathbf{U}_{i,B}(r,y)\sin(k_i\phi) \tag{9}$$

$$\mathbf{U}_{i2}(r,\phi,y) = \mathbf{U}_{i,A}(r,y)\sin(k_i\phi) - \mathbf{U}_{i,B}(r,y)\cos(k_i\phi) \tag{10}$$

By inserting the relation $\theta = \phi + \chi$ between the azimuts, as displayed in Figure 2 and introducing new modal coordinates $Q_{i1}(t) = q_{i1}(t)\cos(k_i\chi(t)) - q_{i2}(t)\sin(k_i\chi(t))$

and $Q_{i2}(t) = q_{i1}(t)\sin(k_i\chi(t)) + q_{i2}(t)\cos(k_i\chi(t))$, the modal synthesis can be transformed into a new formulation:

$$\begin{aligned}\mathbf{u}(r,\phi(t),y,t) &= \sum_i \left[\mathbf{U}_{i1}(r,\phi(t),y)q_{i1}(t) + \mathbf{U}_{i2}(r,\phi(t),y)q_{i2}(t)\right] \\ &= \sum_i \left[\mathbf{U}_{i1}(r,\theta,y)Q_{i1}(t) + \mathbf{U}_{i2}(r,\theta,y)Q_{i2}(t)\right] \end{aligned} \tag{11}$$

In this formulation, the shape functions $\mathbf{U}_{i1}(r,\theta,y)$ and $\mathbf{U}_{i2}(r,\theta,y)$ expressing the deformations in tangential, axial and radial direction and thereby also the shape functions $\mathbf{W}^{\mathcal{A}}_{i1}(r,\theta,y) = \mathbf{A}_2(\theta)\mathbf{U}_{i1}(r,\theta,y)$ and $\mathbf{W}^{\mathcal{A}}_{i2}(r,\theta,y) = \mathbf{A}_2(\theta)\mathbf{U}_{i2}(r,\theta,y)$ expressing the deformations in the directions of the Cartesian coordinates used in frame $\mathcal{A}$ are constant. Further details to this transformation can be found in [2]. By using this formulation all trigonometric functions $\cos\chi$, $\sin\chi$, $\cos(k_i\chi)$ and $\sin(k_i\chi)$ are eliminated. This allows e.g. a linearisation, which can give a quick overview on the system's behaviour. As an example, the frequency response functions for a rotating wheelset, which is integrated into the bogie of a passenger coach and excited by lateral forces, are shown in Figure 3. The angular velocity of the overturning motion is set to $\dot{\chi} = -v_0/r_0$ using a nominal radius of $r_0 = 0.46$ m. The peaks of the frequency response functions can be related to structural eigenfrequencies of the wheelset. Furthermore, a splitting of the peaks, which is a typical gyroscopic effect, occurs for the modes of $f_0 = 147$ Hz and $k_i = 1$ and of $f_0 = 345$ Hz and $k_i = 2$. The peak related to the umbrella mode of $f = 304$ Hz remains nearly unchanged, because it is a rotational symmetric mode, i.e. $k_i = 0$, which has no spatial orientation.

3 Flexible track

The choice of the track model depends strongly on the purpose of the model. For the modelling of vehicle-track interaction, the motions of the railhead under each wheel are of interest. Therefore, the main focus is in this case on the dynamical receptance of the track, i.e. the motions of the rail head as a reaction to dynamic excitation forces.

A general problem is that the longitudinal dimension of the track is far larger than the length of the vehicle. Especially for high running speeds, the vehicle covers very long distances: At a running speed of $v_0 = 180$ km/h $= 50$ m/s, a distance of $\Delta s = 500$ m is covered within a time-interval of $\Delta t = 10$ s. A track model of such a length would require an enormous computational effort. This problem can be solved by using a track model with a shorter length l_{T} and setting the boundary conditions at the rail's ends equal. Thereby, the whole track model forms a "ring with neglected curvature" so that the vehicle never reaches the end of the track. Such a model has been developed by Ripke in [3]. This track model consists of two flexible rails, which are supported by discrete rigid sleepers. The pads connecting the sleepers to the rails and the underground supporting the sleepers are represented by linear visco-elastic elements. The track model is completely linear so that a modal decomposition is possible. Furthermore, the rail is modelled by a combination of beams and plates to

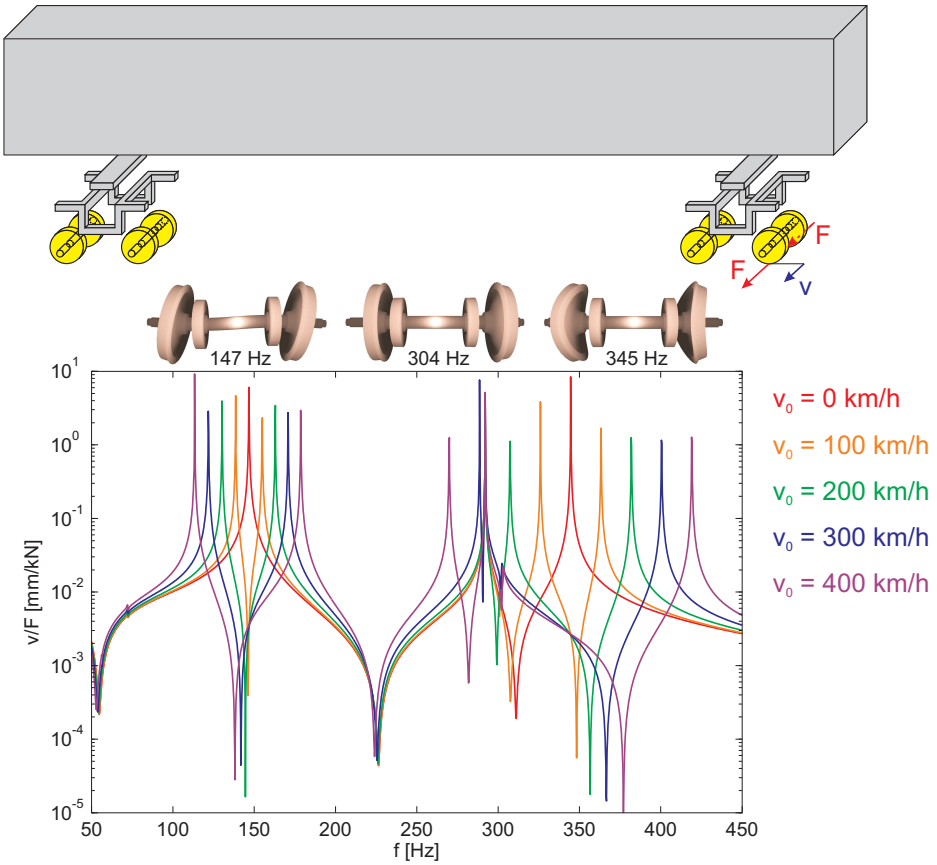

Figure 3: Frequency response function of a passenger coach with rotating wheelsets.

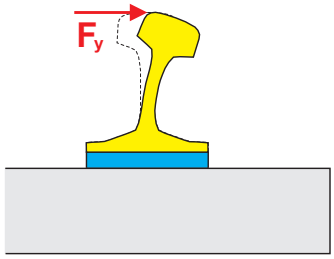

Figure 4: Deformations of the rail's cross section due to lateral contact forces.

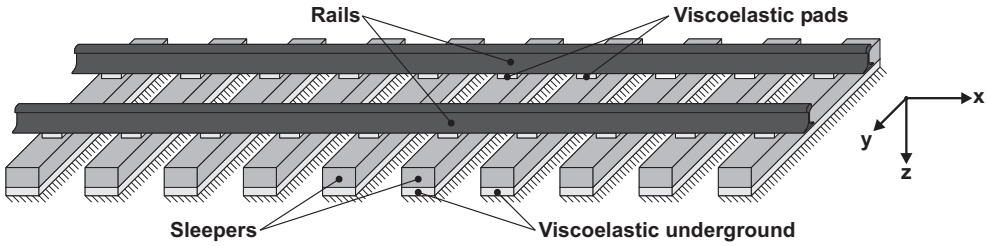

Figure 5: Track model consisting of flexible sleepers supported by discrete rigid sleepers.

take deformations of the cross section into account. The foot of the rail is connected to the sleepers by pads, the web of the rail is comparatively thin and lateral forces applied on the rail head are acting at an eccentric position. Thereby, deformations of the cross section as illustrated qualitatively in Figure 4 can be expected. Since the geometry of the wheel-rail contact can be very sensitive to changes of the relative kinematics, this effect should be taken into account.

An overview of the track model developed here is displayed in Figure 5. Compared to the original model by Ripke it is enhanced in several aspects: In the new track model, the inclination or cant of the rails is taken into account, and distributed springs and dampers are used for the pads instead of the compact elements. While the original rail model from [3] consists of beams and plates to model cross-sectional deformations of the rail, the enhanced track model uses a three-dimensional FE model for the rail. This rail model uses a semi-analytic solution of Navier's equation for a prismatic structure, where the density ρ, the shear modulus G and Poisson's ratio ν are independent on the longitudinal coordinate x:

$$\Delta \mathbf{w} + \frac{1}{1-2\,\nu(y,z)} \mathbf{grad}\,\mathrm{div}\,\mathbf{w} - \frac{\rho(y,z)}{G(y,z)}\ddot{\mathbf{w}} = \mathbf{0} \tag{12}$$

The semi-analytic solution is based on the separation of the longitudinal coordinate x from the coordinates y and z. In the longitudinal direction, the deformation field is described by trigonometric functions depending on x. It can be shown that the

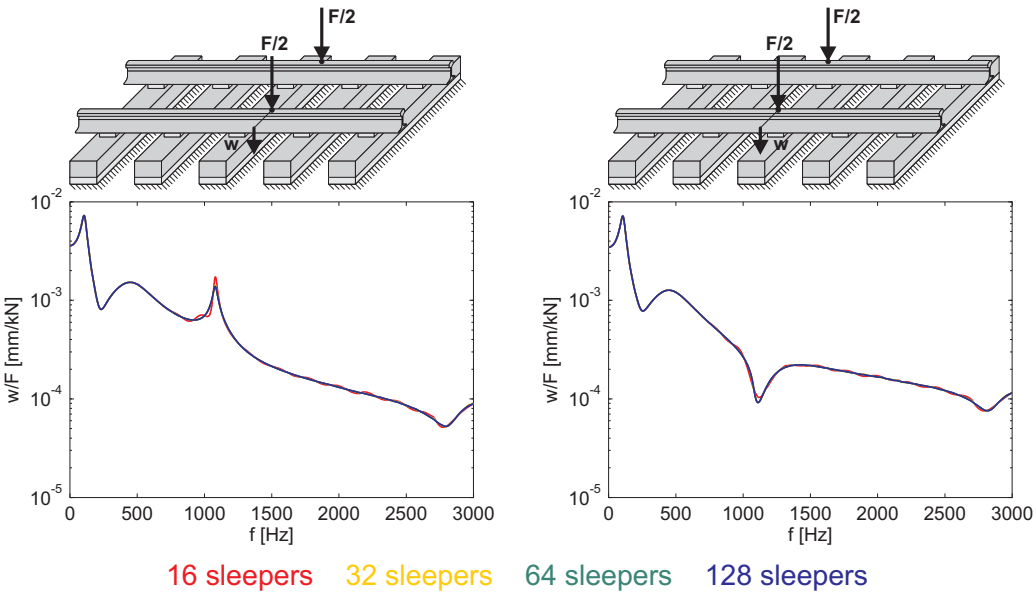

Figure 6: Frequency response functions for symmetric vertical excitation.

following expression is a solution of (12):

$$\mathbf{w} = \begin{bmatrix} U_i(y,z)\sin(\kappa_i x + \alpha_i) \\ V_i(y,z)\cos(\kappa_i x + \alpha_i) \\ W_i(y,z)\cos(\kappa_i x + \alpha_i) \end{bmatrix} \cos(\omega_i t + \beta_i),\ \kappa_i = \frac{2\,\pi\,k_i}{l_\mathrm{T}},\ k_i \in \mathbb{Z} \qquad (13)$$

Due to the semi-analytic solution, an FE discretisation is necessary only for the cross section, which means a considerable reduction of the numerical effort without loss of accuracy. Furthermore, the use of continuous functions depending on x avoids the interpolation, which had already been mentioned in connection with the wheelset.

The question arises how long the track length l_T has to be. As already mentioned, the dynamic receptance behaviour of the track model at the rail head is of main interest. Therefore, the frequency response function for a periodic excitation at the rail head is calculated for different sleeper numbers of $n_{\mathrm{Sl}} = 16$, $n_{\mathrm{Sl}} = 32$, $n_{\mathrm{Sl}} = 64$, and $n_{\mathrm{Sl}} = 128$. Using a sleeper spacing of $\Delta x_{\mathrm{Sl}} = 0.6$ m, these numbers refer to track lengths of $l_\mathrm{T} = 9.6$ m, $l_\mathrm{T} = 19.2$ m, $l_\mathrm{T} = 38.4$ m, and $l_\mathrm{T} = 76.8$ m. In Figure 6, the frequency response functions for a symmetric excitation by vertical forces are displayed. The left diagram shows the results for the excitation in the middle between two sleepers, the right diagram those for the excitation above one sleeper. In the left diagram, the peak resulting from the so-called pinned-pinned mode can be seen at 1100 Hz: For this mode, the nodes of the rails are located above the sleepers. Since the pads connecting the rails and the sleepers contribute strongly to the damping of the system, this mode is only weakly damped. In both diagrams, it can be seen, that the curves for 32, 64 and 128 sleepers are nearly identical, while only the curve for 16 sleepers deviates slightly from the other curves. Apparently, a model consisting of 32 sleepers already gives a very good approximation for a very long track. In Fig-

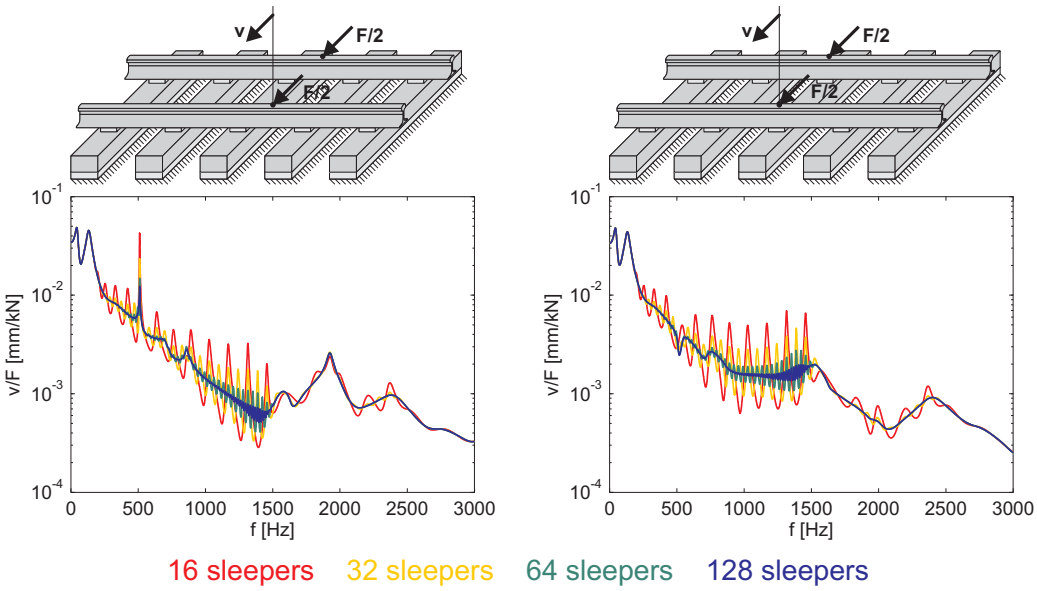

Figure 7: Frequency response functions for lateral excitation.

ure 7, the frequency response functions for an antimetric excitation by lateral forces are displayed. Again, peaks related to a pinned-pinned mode can be observed, in this case at 510 Hz and at 1920 Hz. The convergence of the frequency response functions depending on the sleeper number is slower compared to the case of vertical excitation: For 16 sleepers, distinct peaks can be observed, especially in the range between 200 Hz and 1600 Hz. If the sleeper number is doubled, the peaks become smaller and new peaks appear between the old ones, so that the curves become smoother with increasing sleeper numbers. The peaks result from waves travelling through the "ring" and return to the point of excitation. If the track model is longer, the damping of the waves is higher. Furthermore, new eigenfrequencies causing new peaks occur if the length of the structure is increased. – The question arises, why the convergence of the frequency response functions is quite fast in the case of vertical excitation, while it is slower for lateral excitation. The main contribution to the system's damping results from the pads, while the internal damping of the rails is much less. A vertical motion of the rail including the foot causes a compression or an expansion of the pads, which has a damping effect on the whole system. In the case of lateral excitation, the rail can perform a motion containing a lateral motion, a torsion and a deformation of the cross section. Thereby, the motions of the rail foot are smaller leading to smaller deformations of the pads, which contribute to the damping.

4 Wheel-rail contact

In the multi-body formalism, the wheel-rail contact is represented by a force element. The inputs of such a force element are the relative kinematics of two points, each one

belonging to one of the two bodies, between which the element acts. The outputs are the resulting forces and torques, which are applied to the bodies at the aforementioned points.

In the wheel-rail contact, stresses occur, which are related to deformations in the contact. However, the region, in which these stresses have a direct influence on deformations, is small compared to the main dimensions of the wheelset and the rail. Therefore, deformations occurring in the contact region are considered as local deformations in contrast to global deformations like e.g. bending of the wheelset or the rail and are treated separately.

A very widely used theory for the calculation of contact forces is the Hertzian theory, which assumes elliptical contact areas. By using coefficients stored in tables this theory has a high computational efficiency. However, for several combinations of wheel and rail profiles non-elliptic contact areas occur, which cannot be described by the Hertzian theory. One possibility to treat this problem is to estimate the contact area and the stress distribution by applying certain characteristics of the Hertzian theory to the nonelliptic contact. Several methods of this kind are presented in the survey paper by Piotrowski and Chollet [4]. Another possibility is the numerical solution of the contact mechanics problem, which will be used for the contact model developed here.

The wheel-rail contact model uses a Boundary Element method for the formulation of the contact equations. The fundamentals of this contact modelling are given by Kalker in [5]. The basic assumptions for this model are:

- The wheel and the rail are modelled as half-spaces, i.e. the contact area is small compared to the main dimensions of the wheel and the rail.
- The materials of wheel and rail are linear elastic.
- The shear modulus G and Poisson's ratio are equal for the wheel and the rail.

The relation between the stress acting at the surface of the halfspace on the one hand and the deformations at the surface on the other hand is given by the equations of Boussinesq and Cerruti. If the material parameters G and ν are equal for both bodies, the equations describing the normal stresses and deformations are decoupled from the ones for the tangential stresses and deformations. For pressure described by the distribution $p(x, y)$ acting on the surfaces of the bodies in contact, the resulting normal deformation $w(X, Y)$, i.e. the sum of the deformations of both bodies, is given by:

$$w(X,Y) = \frac{1-\nu}{\pi\, G} \int_A \frac{p(x,y)}{R} \mathrm{d}A \;, \quad R = \sqrt{(X-x)^2 + (Y-y)^2} \tag{14}$$

For a tangential stress field described by $\tau_1(x, y)$ and $\tau_2(x, y)$, the tangential deforma-

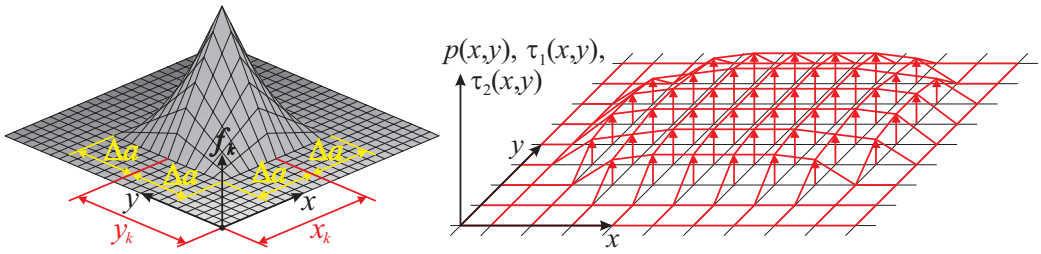

Figure 8: Local bilinear function f_k (left), discretisation of the stresses (right).

tions $u_1(X,Y)$ and $u_2(X,Y)$ at the surface are given by:

$$\begin{aligned} u_1(X,Y) &= \frac{1}{\pi\, G}\int_A \left[\frac{1-\nu}{R}+\frac{(X-x)^2\nu}{R^3}\right]\tau_1(x,y)\mathrm{d}A \\ &\quad +\frac{\nu}{\pi\, G}\int_A \frac{(X-x)(Y-y)}{R^3}\tau_2(x,y)\mathrm{d}A \qquad (15) \\ u_2(X,Y) &= \frac{\nu}{\pi\, G}\int_A \frac{(X-x)(Y-y)}{R^3}\tau_1(x,y)\mathrm{d}A \\ &\quad +\frac{1}{\pi\, G}\int_A \left[\frac{1-\nu}{R}+\frac{(Y-y)^2\nu}{R^3}\right]\tau_2(x,y)\mathrm{d}A \qquad (16) \end{aligned}$$

For the discretisation of the problem, a grid is defined which uses equal spacing Δa in both directions. Thereby, the coordinates of the i-th grid point are given by:

$$x_i = n_{x,i}\,\Delta a,\ y_i = n_{y,i}\,\Delta a,\ n_{x,i}, n_{y,i} \in \mathbb{Z} \qquad (17)$$

The distributions of the stresses $\tau_1(x,y)$, $\tau_2(x,y)$ and $p(x,y)$ are discretised by superposing local bilinear functions $f_k(x,y)$, which are scaled by the values of the stresses at the grid points, as shown in Figure 8. Thereby, the stress field is expressed by:

$$\begin{bmatrix}\tau_1(x,y)\\ \tau_2(x,y)\\ p(x,y)\end{bmatrix} = \sum_k \begin{bmatrix}\tau_1(x_k,y_k)\\ \tau_2(x_k,y_k)\\ p(x_k,y_k)\end{bmatrix} f_k(x,y) = \sum_k \begin{bmatrix}\tau_{1,k}\\ \tau_{2,k}\\ p_k\end{bmatrix} f_k(x,y),\ f_k(x_k,y_k)=1 \qquad (18)$$

By inserting the discretised stress distributions into the Boussinesq equations, the deformations at the grid points, i.e. $u_{1,i} = u_1(x_i,y_i)$, $u_{2,i} = u_2(x_i,y_i)$ and $w_i = w(x_i,y_i)$, can be calculated. This leads to two systems of linear equations:

$$\mathbf{H}_{33}\,\mathbf{p} = \mathbf{w} \qquad (19)$$

$$\begin{bmatrix}\mathbf{H}_{11} & \mathbf{H}_{12}\\ \mathbf{H}_{12} & \mathbf{H}_{22}\end{bmatrix}\begin{bmatrix}\mathbf{t}_1\\ \mathbf{t}_2\end{bmatrix} = \begin{bmatrix}\mathbf{u}_1\\ \mathbf{u}_2\end{bmatrix} \qquad (20)$$

The vectors $\mathbf{t}_1$, $\mathbf{t}_2$ and $\mathbf{p}$ contain the stresses $\tau_{1,k}$, $\tau_{2,k}$ and p_k occuring at the grid points, respectively. The deformations $u_{1,i}$, $u_{i,2}$ and w_i are arranged in the vectors $\mathbf{u}_1$, $\mathbf{u}_2$ and $\mathbf{w}$.

For the normal contact problem, the interpenetration $\delta(x_i, y_i) = \delta_i$ between the undeformed surfaces of wheel and rail is determined at the grid points. If a point belongs to the contact area, the pressure is positive and the deformation is compensating the interpenetration. If a point lies out of the contact area, the deformation is larger than the interpenetration, and the pressure vanishes:

$$\text{inside the contact area} \quad : \quad \delta(x_i, y_i) - w(x_i, y_i) = 0 \wedge p(x_i, y_i) > 0 \tag{21}$$

$$\text{outside the contact area} \quad : \quad \delta(x_i, y_i) - w(x_i, y_i) < 0 \wedge p(x_i, y_i) = 0 \tag{22}$$

Because of the second condition (22) the order of the problem is not known at the beginning of the calculation. Therefore, the application of the standard solution for a system of linear equations using a decomposition of the matrix into a lower and an upper triangular matrix is not very efficient in this case. A more efficient method to solve this problem is the application of the Gauss-Seidel method, which had already been presented by Vollebregt in [6] for solving contact problems. By transforming the i-th equation of the system of linear equations, an iteration scheme is obtained:

$$\sum_{j=1}^{n} H_{ij}^{(33)} p_j = \delta_i \Rightarrow p_i^{(k+1)} = \frac{1}{H_{ii}^{(33)}} \left[\delta_i - \sum_{j=1}^{i-1} H_{ij}^{(33)} p_j^{(k+1)} - \sum_{j=i+1}^{n} H_{ij}^{(33)} p_j^{(k)} \right] \tag{23}$$

Here, $p_i^{(k)}$ is the k-th approximation for the pressure p_i. Using this iteration, the condition (22) can be taken into account very easily: If the iteration scheme (23) yields a negative value $p_i^{(k+1)} < 0$, the value is set to $p_i^{(k+1)} = 0$.

To solve the tangential contact problem, the relative velocities in the contact have to be considered. The actual velocities $v_1(x, y)$ and $v_2(x, y)$ in the contact are obtained by superposing the velocities $v_{0,1}(x, y)$ and $v_{0,2}(x, y)$ of the entire bodies and the velocities $v_{d,1}(x, y)$ and $v_{d,2}(x, y)$ resulting from the deformations:

$$v_I(x, y) = v_{0,I}(x, y) + v_{d,I}(x, y), \; I = 1, 2 \tag{24}$$

The velocities $v_{0,1}(x, y)$ and $v_{0,2}(x, y)$ only depend on the input kinematics of the wheel-rail contact element, therefore they are considered as given. The deformational velocities can be approximated by using the wanted deformations $u_1(x, y) = u_1(x, y, t = t_0)$ and $u_2(x, y, t = t_0)$ at the current time $t = t_0$ and the deformations $u_1^*(x, y) = u_1(x, y, t = t_0 - \Delta t)$ and $u_2^*(x, y) = u_2(x, y, t = t_0 - \Delta t)$ at an earlier time $t = t_0 - \Delta t$.

$$v_I(x, y) \approx v_{0,I}(x, y) + \frac{u_I(x, y) - u_I^*(x, y)}{\Delta t}, \; I = 1, 2 \tag{25}$$

Here, the deformations $u_1^*(x, y)$ and $u_2^*(x, y)$ are also considered being given. If adhesion is assumed at the i-th point, the velocities $v_1(x_i, y_i)$ and $v_2(x_i, y_i)$ vanish, which leads to the following conditions:

$$u_{I,i} = u_I(x_i, y_i) = u_I^*(x_i, y_i) + \Delta t \cdot v_{0,I}(x_i, y_i), \; I = 1, 2 \tag{26}$$

By transforming the equations (20) into a scheme analogous to (23) and inserting the condition (26), an iteration for $\tau_{1,i}^{(k)}$ and $\tau_{2,i}^{(k)}$ is obtained. However, the stresses $\tau_{1,i}$ and $\tau_{2,i}$ are limited by the transmittable stress, which can be expressed by the following condition:

$$\sqrt{\tau_1(x,y)^2 + \tau_2(x,y)^2} = |\tau(x,y)| \leq \mu\, p(x,y) \tag{27}$$

If the resulting stress obtained from the iteration doesn't exceed the transmittable stress, i.e. $\left|\tau_i^{(k+1)}\right| \leq \mu\, p_i$, the assumption of adhesion is true, otherwise sliding actually occurs. In this case, the tangential stress are acting in the opposite direction of the relative velocity and the resulting stress is equal to the transmittable stress:

$$\begin{aligned} &\tau_1(x,y) = -C\, v_1(x,y),\ \tau_2(x,y) = -C\, v_2(x,y),\ C > 0 \\ &\quad \Rightarrow \tau_1(x,y)\, v_2(x,y) - \tau_2(x,y)\, v_1(x,y) = 0 \wedge \sqrt{\tau_1(x,y)^2 + \tau_2(x,y)^2} = \mu\, p(x,y) \end{aligned} \tag{28}$$

Also here, the Gauss-Seidel method provides an efficient way to take this nonlinear condition into account, as presented by Vollebregt in [6]. – In the presented wheel-rail contact model, stationary rolling is assumed. The particles are moving through the contact area in the negative x-direction. By choosing the time interval $\Delta t = \Delta a / v_0$, the earlier deformation states $u_1^*(x,y)$ and $u_2^*(x,y)$ are equal to the current deformation states $u_1(x - \Delta a, y)$ and $u_2(x - \Delta a, y)$, respectively:

$$u_1^*(x,y) = u_1(x - \Delta a, y),\ u_2^*(x,y) = u_2(x - \Delta a, y) \tag{29}$$

From the calculated stresses, the resulting forces and torques with respect to two certain points, the one on the wheel rim, the other one on the rail head, are determined. By the torques, lateral shifts of the contact area are taken into account.

5 Vehicle-track system

The refined components, i.e. the model of the flexible rotating wheelsets, the flexible track model and the wheel-rail contact model, are integrated into an entire vehicle-track system. An overview of the system is given in Figure 9. The vehicle-track system describes a passenger coach, which is running on a straight track. The passenger coach has two bogies, each one equipped with two wheelsets. The carbody, the bogie frames and the bolsters are modelled as rigid bodies, while all four wheelsets are described as flexible bodies. Each bogie frame and each wheelset can perform all six rigid-body motions. The car body can perform all three rotations, i.e. the roll motion, the pitch motion and the yaw motion, and the lateral and the vertical translation, while for the longitudinal translation a constant running speed v_0 is set. The bolsters can only perform yaw motions relative to the car body. Each bogie frame is connected to the wheelset and the bolster by linear springs and dampers. Between the car body and each bolster, a dry friction element, which provides the yaw damping, acts. The

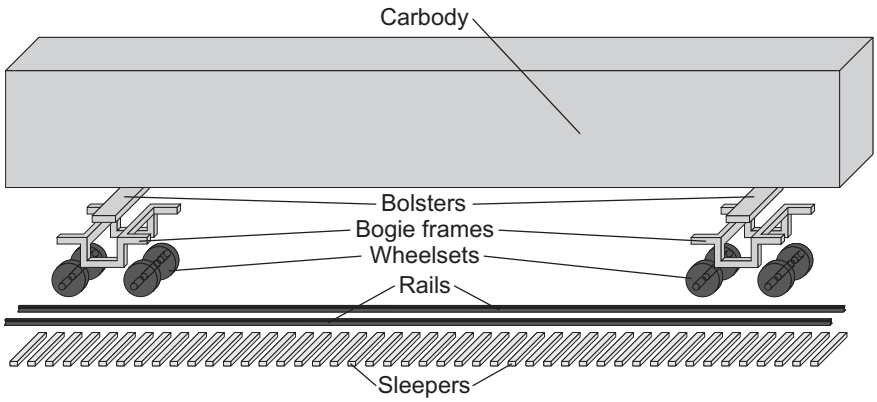

Figure 9: Bodies of the vehicle-track system; dark bodies are modelled as flexible bodies.

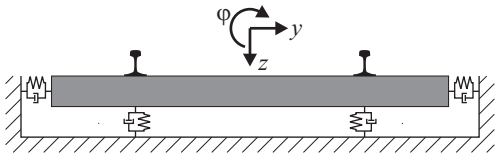

Figure 10: Simple track model.

parameters are taken from the works of Diepen [7] and Kim [8]. As mentioned in chapter 3, the track includes two flexible rails, which are supported by 128 sleepers. For the rails, the profile UIC60 is chosen. The rail inclination or cant is set to 1/40. The whole vehicle-track model contains eight wheel-rail contacts. Here, the profiles S1002 for the wheel and UIC60 for the rail are used. For the calculations presented in this paper, a friction coefficient of $\mu = 0.3$ is set. For the discretisation of the contact problem, a spacing of $\Delta a = 0.75$ mm is used.

With this model, two scenarios are studied: The centred running and the "unstable" hunting of the vehicle. In both cases, no disturbances, i.e. track irregularities, deviations of the profiles or unbalances in the wheelsets, are taken into account. Although the considered scenarios are idealised, they give an insight into the system's behaviour and can be used as a plausibility check of the model. To study the influences of the flexibilities of the wheelset and of the track, four different variants of the model are used, in which the flexibilities are either taken into account or neglected. The wheelset may be modelled as a rigid body, a completely rigid track would however be unrealistic. Therefore, simple track elements as displayed in Figure 10, each one supporting one wheelset, are used for the comparison. The track element consists of a rigid body, which can perform a lateral motion y, a vertical motion z and a roll motion φ. The rigid body is connected to the environment by linear springs and dampers. Model configurations using these track elements will be called "rigid rails". Altogether, four different variants of the vehicle-track model are possible:

- Model *RR*: Rigid wheelsets, rigid rails
- Model *FR*: Flexible wheelset, rigid rails
- Model *RF*: Rigid wheelsets, flexible rails
- Model *FF*: Flexible wheelsets, flexible rails

All results, which will be presented in the following, refer to the leading wheelset of the leading bogie. For the investigation of the wheel-rail contact, the right contact of this wheelset is considered.

5.1 Centred running

In the case of the centred running, the lateral displacement y as well as the roll angle φ and the yaw angle ψ of the wheelsets, the bogie frames and the carbody are zero. The running speed is set to $v_0 = 200$ km/h. In the case of the model *RR*, a stationary state is calculated. For the model *FF*, a weak oscillation due to the sleeper passing occurs. Therefore, the amplitude of the vertical force Q fluctuates between $Q = 59$ kN and $Q = 60.8$ kN, which is very weak.

The geometry of the wheel-rail contact and the profile of the pressure distribution is displayed in Figure 11. The influence of the deformations of wheelset and rail on the contact geometry itself are hardly visible. However, the slight change of the contact geometry causes a considerable change of the pressure distribution, which is also illustrated in Figure 12. For the model *RR*, two maxima of the pressure distribution occur. For the model *FF*, the left maximum shrinks drastically and nearly vanishes, while the right maximum slightly increases. An explanation for this effect may be derived from Figure 15. The vertical forces, i.e. the wheel-rail forces acting at the wheel rims and the forces transmitted between the bearings and the journals, cause a bending of the wheelset, especially of the wheelset's axle. This leads to a positive camber angle of the wheels. For the model *RR*, the relative angle α between the wheel rim and the rail head is $\alpha = 25$ mrad, resulting from the rail cant of 1/40. Due to the bending, the angle is changed to $\alpha \approx 26$ mrad. Thereby, the left part of the contact area is unloaded, while the loading increases in the right part.

The wheelset performs a large rolling motion around its axis of symmetry. Because of the small inclination of the contact area relative to the axis of symmetry, a small spin occurs in the contact. This explains the concentric distribution of the tangential stresses shown in Figure 13. The sliding occurs at the trailing edge of the contact patch, the few single points indicating sliding at the leading edge are results of discretisation errors. The distribution of the friction power density P_F/A resulting from the sliding is displayed in Figure 14. Also here, a considerable impact of the deformations can be seen: The distribution obtained for the model *RR* shows two maxima, a larger one of $P_F/A = 13$ W/mm^2 in the left part of the contact patch and a smaller one of $P_F/A = 7$ W/mm^2 in the right part. For the model *FF* the left maximum is

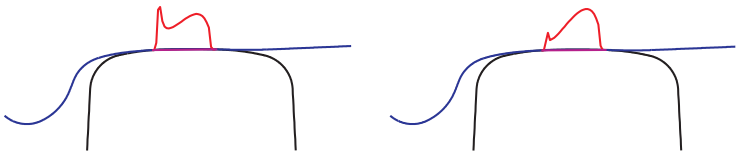

Figure 11: Contact geometry; left: model *RR*, right: model *FF*.

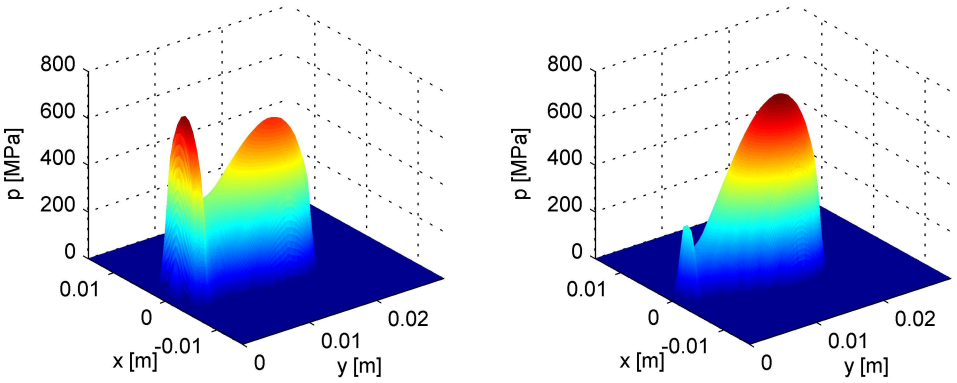

Figure 12: Distribution of the normal pressure; left: model *RR*, right: model *FF*.

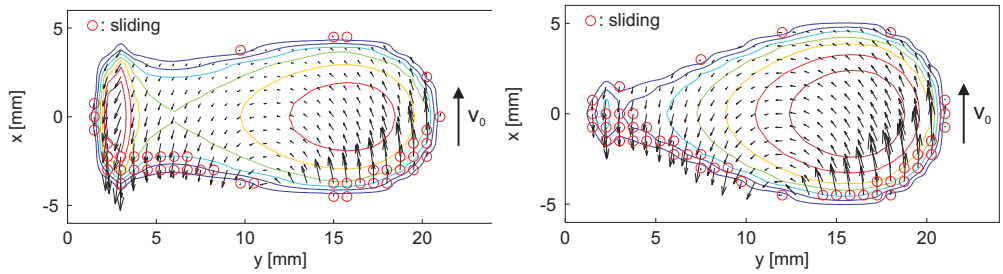

Figure 13: Distribution of the tangential stresses; left: model *RR*, right: model *FF*.

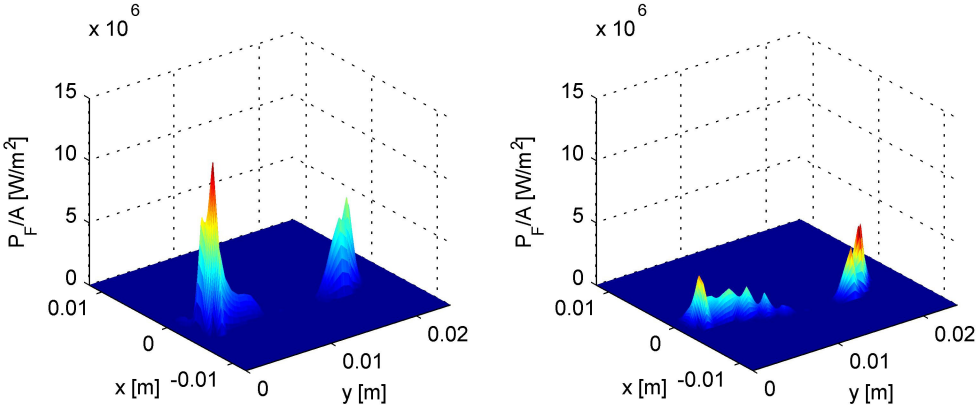

Figure 14: Distribution of the frictional power density; left: model *RR*, right: model *FF*.

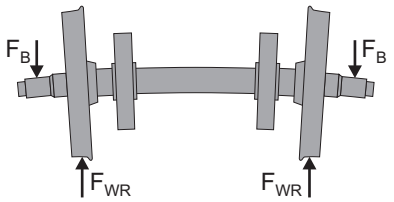

Figure 15: Bending of the wheelset (qualitative scheme) due to the vertical wheel-rail forces F_{WR} and the vertical forces F_B transmitted by the bearings to the journals.

considerably reduced to $P_F/A = 4$ W/mm^2, while the right maximum is slightly diminished to $P_F/A = 5$ W/mm^2. As observed in Figure 12, the pressure p in the left part of the contact patch is drastically reduced for the model *FF*. The reduced pressure also leads to a reduction of the transmittable tangential stress $\tau_{max} = \mu\, p$.

5.2 Hunting

Below a certain running speed, the so-called critical speed $v_{0,crit}$, lateral motions of the vehicle die out and the vehicle centres itself within the track. If the vehicle runs faster than the critical speed, motions excited by disturbances may not die out, but a permanent combined lateral and yaw motion, the so-called hunting motion occurs. Although this motion is stable in the mathematical sense, it is often called "unstable" hunting. Since this motion can lead to high lateral wheel-rail forces, which can damage the track and increase the risk of derailment, this scenario should be avoided in regular operation. Therefore railway vehicle are usually designed in such a way that the critical speed is distinctly higher than the maximum operational speed.

Although the scenario of "unstable" hunting is not desired in regular operation, it can be used for studying the behaviour and checking the plausibility of the model. In Figure 16 the phase portraits for the lateral motion y_{WS1} for the centre of the leading wheelset in the leading bogie are displayed. The calculations were carried out for all four model variants *RR*, *RF*, *FR* and *FF*.

The comparison of the diagrams shows that the amplitudes of the lateral displacements become larger, if the flexibilities of the wheelsets and the track are taken into account. In particular the flexibility of the wheelsets causes a distinct increase of the amplitudes. This can be explained in the following way: If the wheel flange hits the rail head, large lateral forces occur, which shift the wheel rim towards the wheelset's centre. Thereby, a larger lateral displacement of the centre occurs.

Furthermore, the diagram obtained for the model *RR* shows sharp bends of the curves at $y_{WS} \approx 6$ mm and $y_{WS} \approx -6$ mm. This effect is caused by the wheel flange: If the wheel flange hits the rail head, large lateral forces occur, which decelerate the wheelset's lateral motion. If the flexibility of the wheelset is taken into account, the wheelset as a complete structure is softer than the comparatively stiff wheel-rail contact. Thereby, the impact of the flange is cushioned, which leads to smoother curves.

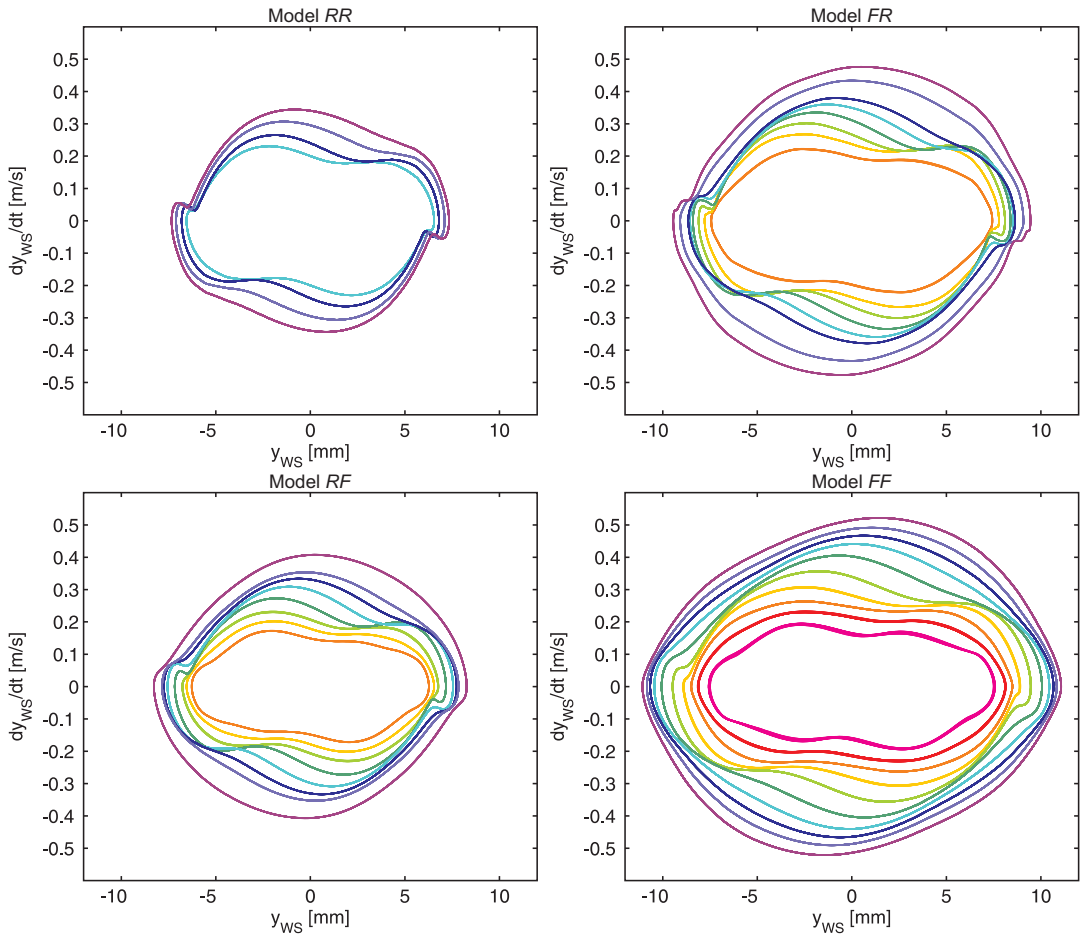

Figure 16: Phase portraits for the lateral motion y_{WS} of the wheelset's centre.

The cushioning effect of the flexible track is even more distinct: While a very weak influence of the contact between wheel lange and rail head can be seen for the model *FR* at $v_0 = 420$ km/h, the curves obtained with the model *RF* are very smooth and the sharp bends vanish completely. If the track elements displayed in Figure 10 are used, the entire rigid body of the element has to be accelerated, if the flange hits the rail head. In the case of the flexible track model, the sleepers are connected to the rails by the pads allowing relative motions. Thereby, the lateral forces don't have to accelerate such a high mass.

For the models *FR* and *RF* the curves for $v_0 = 330$ km/h and $v_0 = 340$ km/h are not available, because for these models no permanent hunting occurs at these running speeds. For the same reason, the curves for $v_0 = 330$ km/h up to $v_0 = 380$ km/h are missing for the model *RR*. This indicates that the flexibilities have an impact on the critical speed $v_{0,crit}$. Apparently, the deformations have an influence on the creepages in the contact and thereby on the contact forces so that the "unstable" hunting starts at lower running speeds.

In Figure 17 the wheel-rail contact geometry and the pressure distribution in the contact depending on the lateral displacement y_{WS} is displayed for the models *RR* and *FF*, obtained for a running speed of $v_0 = 420$ km/h. It can be seen that also in the case of hunting the flexibilities of the wheelsets and the track have a distinct impact on the stress distribution occurring in the wheel-rail contact. Furthermore, if the displacement is increased from $y_{WS} = 9$ mm up to $y_{WS} = 11$ mm, the contact geometry and the pressure distribution are hardly changed. This indicates that the increase of the amplitude is in fact mainly caused by structural deformations of the wheelset and the track.

6 Conclusion

The wheelsets, the rails and the wheel-rail contact are the key components for the vehicle-track interaction. Therefore, refined models of these components are developed. The main problem related to the modelling of a rotating wheelset as a flexible body are the wheel-rail forces circulating around the wheel. The shape functions describing the deformation of the wheelset are expressed by trigonometric functions providing a simpler evaluation than a piecewise interpolation. If the wheelset is assumed to be a rotational symmetric structure, several characteristics of the eigenmodes of such a structure can be exploited to simplify the calculation without loss of accuracy. For the modelling of the track, the large dimension of the track is the main difficulty. Since for vehicle-track simulations the receptance behaviour of the track, i.e. the motions of the rail head as a reaction to the excitation by wheel-rail forces, are of main interest, the numerical effort can be drastically reduced by using a ring-shaped track model and neglecting its curvature. However, the influence of the length of the track model on the receptance behaviour has to be investigated carefully to obtain a sufficient approximation for the dynamic behaviour of a very long track. The wheel-rail contact model is based on an iterative solution of the contact equations obtained from

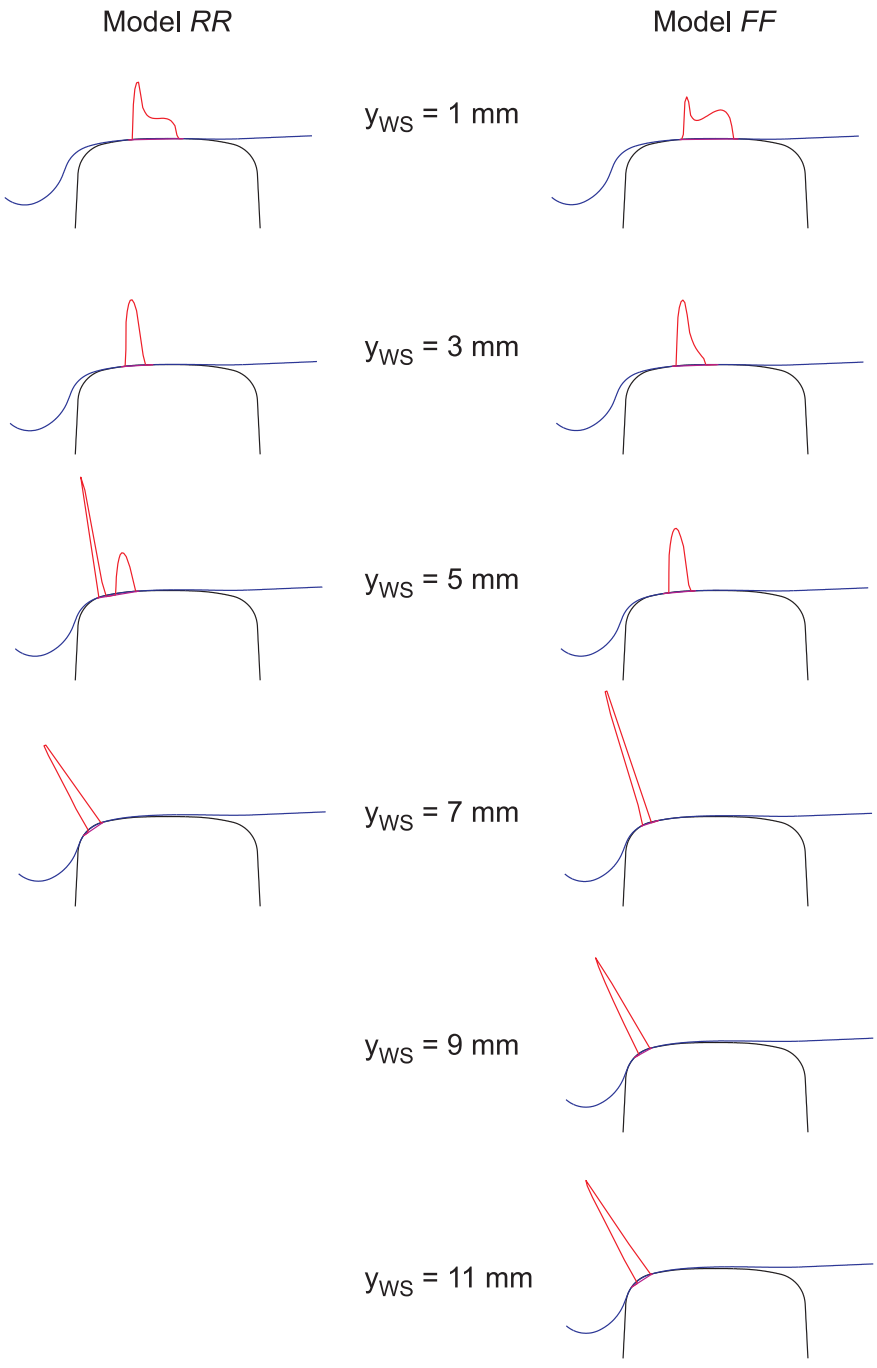

Figure 17: Contact geometry and pressure distribution depending on the lateral motion y_{WS} of the wheelset's centre.

a Boundary Element model. The refined components are integrated into the model of a passenger coach running on a straight track. The influences of the flexibilities of the wheelsets and the track are investigated in two idealised scenarios.

Already in the "unspectacular" case of undisturbed centred running, a distinct impact of the structural deformations of the wheelsets and the track on the wheel-rail contact can be seen: Although the change of the relative kinematics of the wheel rim and the rail head caused by the structural deformations is small, the distributions of the stresses and the friction power density, which is relevant for the wear, are noticeably changed. As an example for a highly dynamic interaction of vehicle and track, the scenario of "unstable" hunting is investigated. It turns out that the flexibilities of the wheelsets as well as of the track have a distinct impact on the running behaviour. This underlines the necessity of a consistent modelling, i.e. all components should have a similar grade of detailing. The increased numerical effort for a detailed contact model only makes sense, if the input for the contact model is taken from refined models of the wheelset and the track. Altogether, the enhanced components and the refined vehicle-track model including these components enable a detailed, but also efficient modelling. This provides a suitable base for investigations of phenomena like noise and wear.

References

[1] L.D. Landau and E.M. Lifshitz, "Theory of elasticity", Butterworth-Heinemann, Oxford, 1986.

[2] A. Heckmann, S. Hartweg and I. Kaiser: An Annular Plate Model in Arbitrary Lagrangian-Eulerian Description for the DLR FlexibleBodies Library, Proceedings of the 8th International Modelica Conference, Dresden, 20-22 March 2011.

[3] B. Ripke, "Hochfrequente Gleismodellierung und Simulation der Fahrzeug-Gleis-Dynamik unter Verwendung einer nichtlinearen Kontaktmechanik", Fortschritt-Berichte Reihe 12, VDI-Verlag, Düsseldorf, 1995.

[4] J. Piotrowski and H. Chollet, "Wheel-rail contact models for vehicle system dynamics including multi-point contact", Vehicle System Dynamics, 43, 455-483, June 2005.

[5] J. J. Kalker, "Three-dimensional elastic bodies in rolling contact", Kluwer Academic Publishers, Dordrecht, 1990.

[6] E. A. H. Vollebregt, "A Gauss-Seidel type solver for special convex programs, with application to frictional contact mechanics", Journal of Optimization Theory and Applications, 87, 47-67, October 1995.

[7] P. Diepen, "Horizontaldynamik von Drehgestellfahrzeugen: Berechnung und Optimierung des Laufverhaltens von schnellfahrenden Reisezugwagen mit konventionellen Laufwerken", Dissertation, TU Braunschweig, 1991.

[8] K.-H. Kim, "Verschleissgesetz des Rad-Schiene-Systems", Dissertation, RWTH Aachen, 1991.